

# Investigating the risks of debris-generating ASAT tests in the presence of megaconstellations

Sarah Thiele<sup>1</sup> and Aaron C. Boley<sup>1</sup>

<sup>1</sup>*University of British Columbia, Department of Physics and Astronomy*

## ABSTRACT

The development of large constellations of satellites (i.e., so-called megaconstellations or satcons) is poised to increase the number of LEO satellites by more than an order of magnitude in the coming decades. Such a rapid growth of satellite numbers makes the consequences of major fragmentation events ever more problematic. In this study, we investigate the collisional risk to on-orbit infrastructure from kinetic anti-satellite (ASAT) weapon tests, using the 2019 India test as a model. We find that the probability of one or more collisions occurring over the lifetime of ASAT fragments increases significantly in a satcon environment compared with the orbital environment in 2019. For the case of 65,000 satellites in LEO, we find that the chance of one or more satellites being struck by ASAT fragments of size 1 cm or larger is about 30% for a single test. Including sizes down to 3 mm in our models suggests that impacts will occur for any such event. The heavy commercialization of LEO demands a commitment to avoiding debris-generating ASAT tests.

## 1. INTRODUCTION

On March 27th 2019, India conducted its first successful anti-satellite (ASAT) test. In this operation, code-named ‘Mission Shakti’, a modified anti-ballistic missile interceptor was launched by India’s Defence Research and Development Organization (DRDO) to destroy a 740 kg satellite, Microsat-R [1]. This event placed India among the three other countries with demonstrated direct ascent ASAT capabilities – United States, Russia and China [2].

The mission was implemented with the intent to minimize the amount of long-lasting debris generated by the impact, and thus avoid substantially increasing the risk to crewed space activities, as well as avoid creating a dangerous debris field like the 2007 Chinese ASAT test. In this vein, the DRDO conducted the test when the target satellite was at a low altitude of 283 km. The satellite was also a relatively small Indian communications satellite, with a surface area of about two square metres [3].

Despite these efforts, more than four months later, there were still 57 tracked and catalogued debris in orbit [4]. Ten of those 57 fragments had apogee altitudes greater than 1000 km, and some as high as 1730 km, spanning the majority of LEO’s altitude range and thus endangering most LEO spacecraft, including the International Space Station. It is important to recall that this is only the tracked and catalogued fragments. Modelling suggests [5] that the number of debris fragments created by Mission Shakti with a size larger than 1 mm may have been of order  $10^5$  – sizes that still could cause non-negligible damage.

In addition to the risks associated with a direct collision, any resulting fragmentation has the possibility of prompting multiple further fragmentations [6]. Even if a collisional cascade does not develop, fragmentation events are problematic for the safe operation of spacecraft in orbit.

The development of substantial orbital infrastructure, such as ‘satcons’ (i.e., so-called megaconstellations), makes the negative consequences of debris-generating ASAT tests much more acute. SpaceX already has 1645 satellites for its Starlink satcon in orbit<sup>1</sup>, with the potential to grow to 42,000 if the first and second generation configurations are combined [7, 8, 9, 10]. Another system, OneWeb, has 288 satellites in orbit<sup>2</sup>, which could increase to 7,000 by the end of their phase 2 launches [11]. These substantial changes in the number of spacecraft in LEO create a need for risk evaluation from a cumulative perspective. While the collision probability between a debris fragment and a single satellite may be low, the integrated probability of impact over an entire system could be non-negligible.

In this study, we explore the collisional risk posed by an ASAT weapon test, similar to that conducted by India in 2019, but with satellites in satcons numbering 65,000 in total.

<sup>1</sup>Based on Celestrak (<https://celestrak.com/>), as of 23 August 2021.

<sup>2</sup>ibid.

## 2. METHODS

We use the astrodynamics code REBOUND [12] to integrate model ASAT-caused debris fragments through satellite density fields in order to assess the probability that the ASAT test will lead to one or more collisions with a satellite, under different scenarios. These density fields are built using public satellite information, as well as proposed satcon configurations. Only collisions between the integrated ASAT debris and satellites are considered, i.e., satellite-satellite and impacts from the existing debris field are excluded to focus specifically on the effects of ASAT testing.

Details regarding the satellite fields are given below. In brief, a satellite distribution is selected and the satellites in that distribution are time-averaged along their orbits. LEO is divided into azimuthally symmetric grid cells, according to altitude and co-latitude. Then, the altitude and co-latitude positions of the satellites along their orbits are used to assign weighted densities to the grid cells, such that a satellite's contribution to a grid cell depends on the time the satellite spends passing through the cell's volume.

Three satellite distributions are used to create density fields for this study: (1) The satellites in LEO as of August 2019<sup>3</sup>, (2) the first 12,000 of SpaceX's Starlink constellation, which will be launched over the next five years, and (3) an environment of 65,000 satellites which include Starlink, OneWeb, Amazon/Kuiper, and GW/StarNet.

### 2.1 REBOUND and REBOUNDx

REBOUND is an open-source flexible N-body integrator that can be used for a wide range of astrophysical and astrodynamical problems. We use the Wisdom-Holman integrator **WIFast** [13] for all simulations presented here, which is well-suited for cases in which orbital perturbations are small. As a consistency check, REBOUND's **IAS15** integrator [12] was also used in preliminary test simulations, which gave statistically indistinguishable results from the **WIFast** runs.

Gas drag is implemented by including a force term

$$\mathbf{F}_d = -\rho \frac{C_D}{2} (A/M) v \mathbf{v} \quad (1)$$

on all fragments. The velocity of a debris particle  $\mathbf{v}$  (and its magnitude  $v$ ) relative to the geocentre is also taken to be the particle's speed through the atmosphere for the purpose of determining drag forces.

The drag coefficient  $C_D$  is held constant at 2.2. The gas density  $\rho$  is a function of altitude only and is determined by linearly interpolating, in log space, between the 2012 tabulated values of the COSPAR International Reference Atmosphere (CIRA) [14]. For objects at altitudes greater than those included in CIRA-2012, the density is linearly extrapolated, in log space, from the two highest entries in the density table. The area-to-mass ratio  $A/M$  is discussed further below.

Collision probability is calculated as a Poisson probability. During each integration timestep  $dt$ , the instantaneous collision probability is determined by

$$p = n\sigma v_{\text{rel}} dt, \quad (2)$$

where  $n$  is the local satellite number density,  $\sigma = 10 \text{ m}^2$  is the assumed satellite cross-section (note that the results are scalable by this value), and  $v_{\text{rel}}$  is the typical relative speed between an ASAT fragment and the satellites in the given grid cell. Because the probability of any one fragment having a collision is small, the cumulative collision probability for the  $i^{\text{th}}$  particle,  $\lambda_i$ , is the sum of an individual particle's instantaneous collision probabilities up until the simulation ends or the particle de-orbits. Finally, the probability of having one or more collisions as a result of the ASAT test is

$$P_{\text{coll}} = 1 - \exp(-\Lambda) \quad (3)$$

for  $N$  debris fragments and  $\Lambda = \sum_i^N \lambda_i$ .

As we use a density field for the satellites, we need a statistical approximation for  $v_{\text{rel}}$ . If all orbits are approximately circular and in the same shell, then the average relative velocity is  $v_{\text{rel}} = \frac{4}{\pi} v_c$ , where  $v_c$  is the local circular orbital speed. Because the fragments can have non-trivial eccentricities, we modify the relative speed to be

$$v_{\text{rel}} \approx \left( \frac{16}{\pi^2} v_\theta^2 + v_r^2 \right)^{1/2}, \quad (4)$$

---

<sup>3</sup>Data obtained from USSPACECOM (<https://www.space-track.org>).

for azimuthal and radial velocity components  $v_\theta$  and  $v_r$ , respectively. At low eccentricities, Equation 4 is the same as that for circular orbits. In tests, the relation gives values that are within about 10% of those determined from Monte Carlo averaging, even for high eccentricity.

## 2.2 Satellite Density Field

In order to simplify the collision probability calculations, we use azimuthally symmetric spherical grid cells to represent an averaged satellite density field. This avoids the need for directly calculating a collision probability between debris fragments and each individual satellite, an expensive computational process.

We assign each cell  $i$  an altitude  $h_i = R_i - R_\oplus$  and a co-latitude  $\theta_i$  value, with respective widths of  $\Delta R = 1$  km and  $\Delta\theta = 1^\circ$ . The inner boundary of the grid has an altitude  $h_{\min} = 300$  km. For the satcon distributions, the upper grid boundary is  $h_{\max} = 1,500$  km. However, the comparison simulation that uses the actual 2019 satellite distribution requires a higher upper boundary, with  $h_{\max} = 2,000$  km. Note that these boundaries are only for defining the satellite density fields.

Because all cells are azimuthally averaged, a single cell has a volume of

$$V_i = 2\pi R_i^2 \Delta R [\cos(\theta_i - \Delta\theta/2) - \cos(\theta_i + \Delta\theta/2)] \quad (5)$$

The orbital parameters for satcons are taken from FCC filings and are listed in Table 1. Each row lists satellites with like altitudes and inclinations.  $N_p$  is the number of unique orbital planes occupied by that particular set of satellites.  $N_{spp}$  is the number of satellites per plane. If this value is 1, each satellite occupies its own orbital plane and the satellites are distributed evenly along their orbits.

For creating the distributions, two different methods are used. For satcons, we distribute the nodes evenly between 0 and  $2\pi$ . The satellites are then placed randomly along their orbits in their respective plane. Due to this randomization, some clumping occurs in the corresponding satellite density fields if only instantaneous positions are used. As a result, the satellites are integrated in REBOUND and the density field is created by averaging multiple snapshots. For both the 65,000 and 12,000 satellite case, we found that 100 snapshots over an orbital period at 600 km altitude is sufficient to smooth out the data.

A different method is used for defining the 2019 satellite density field (i.e., only the satellites that were in orbit at that time). In this case, the orbital parameters for a 2019 satellite distribution are obtained from the USSPACECOM catalogue for August 2019. We only include satellites with perigees below an altitude of 2000 km. This smaller number of satellites ( $\approx 3000$ ) again requires time-averaging for determining a smooth satellite density distribution. In this case, we use each satellite's osculating Keplerian orbits and weight its contribution to each cell by the amount of time it spends in that cell over an orbit.

## 2.3 Simulating a Kinetic ASAT Test

We investigate two methods of simulating debris distributions arising from ASAT testing. The first uses the NASA Standard Breakup Model (NSBM), in which the distributions for fragment velocity kicks and area-to-mass ratios A/M are generated in a probabilistic manner. The second is a simplified approach using a Rayleigh distribution of fragment velocity kicks and a fixed A/M ratio. This is intended to aid in the interpretation of the results and to provide a basic model for easy reproducibility. We discuss these methods in turn.

### 2.3.1 NASA Standard Breakup Model

The NSBM is implemented following [15], which yields probability distributions for parameters that describe debris formed from an explosion or collision. The distributions that we use correspond to the parameterizations for a collision. The choice is intended to better represent the energetics of the India 2019 ASAT test, which used a kinetic kill vehicle rather than an explosive warhead. Distribution parameters can be found in Appendix B of [15].

In the NSBM, the number of fragments with lengths greater than a given characteristic length  $L_c$  is given by:

$$N(> L_c) = 0.1 M_e^{0.75} L_c^{-1.71} \quad (6)$$

$$\text{or } \Delta N = N(> L_0) - N(> L_1) \quad (7)$$

Table 1: Parameters for future LEO satcons, obtained from FCC filings. The number of unique orbital planes is  $N_P$  with number of satellites per plane  $N_{SPP}$ . All satellites in a given row have the same orbital inclination and altitude.

Constellation	$N_P$	$N_{SPP}$	Inc. ( $^{\circ}$ )	Alt. (km)
Starlink Gen1 <sup>a</sup>	2547	1	53	345.6
	2478	1	48	340.8
	2493	1	48	340.8
	72	22	53	550
	72	22	53.2	540
	36	20	70	570
	6	58	97.6	560
	4	43	97.6	560.1
Starlink Gen2 <sup>b</sup>	7178	1	30	328
	7178	1	40	334
	7178	1	53	345
	40	50	96.9	360
	1998	1	75	373
	4000	1	53	499
	12	12	148	604
OneWeb <sup>c</sup>	18	40	87.9	1200
	36	49	87.9	1200
	32	72	40	1200
	32	72	55	1200
GW/StarNet <sup>d</sup>	16	30	85	590
	40	50	50	600
	60	60	55	508
	48	36	30	1145
	48	36	40	1145
	48	36	50	1145
	48	36	60	1145
Amazon/Kuiper <sup>e</sup>	34	34	51.9	630
	36	36	42	610
	28	28	33	590

<sup>a</sup> Approximately 12,000 satellites [7, 8, 9].

<sup>b</sup> Assumes Gen 1 and 2 operating together for a total of approximately 42,000 satellites [10].

<sup>c</sup> Includes phases 1 and 2 for approximately 7,000 satellites [11].

<sup>d</sup> 12,992 satellites, based on multiple ITU filings [17].

<sup>e</sup> 3,236 satellites [18].

where  $M_e$  is the mass of ejected fragments in kilograms,  $L_c$  is the fragment's characteristic length, in metres, and  $L_0$  and  $L_1$  are the lower and upper bounds on a given  $L_c$  bin, respectively.

The fragmenting mass  $M_e$  caused by the collision is dependent on the kill energy per target mass, which is

$$\varepsilon = \frac{1}{2} \frac{m_i}{m_t} v_i^2 = \frac{E_{\text{kill}}}{m_t}, \quad (8)$$

where  $m_i$  and  $m_t$  are the interceptor and target mass, respectively,  $v_i$  is the relative speed between the interceptor and target, and  $E_{\text{kill}}$  is the chosen kill energy. The associated relative impact speed is thus  $v_i = \sqrt{2E_{\text{kill}}/m_i}$ .

If  $\varepsilon < 40 \text{ J/g}$ , it is deemed a 'noncatastrophic' collision, so the target is only cratered, and the ejected mass of fragments is a scaling of the kill energy  $M_e = m_i \left( \frac{v_i}{\text{km/s}} \right)^2$ . If  $\varepsilon \geq 40 \text{ J/g}$ , it is a catastrophic collision and the fragment mass that is ejected is the total mass of the interceptor and target  $M_e = m_i + m_t$ .

We use an effective energy of 130 MJ for India's ASAT test (based, in part, on providing correspondence between Gabbard plots – see below), yielding a catastrophic collision with a fragment mass of  $M_e = 750 \text{ kg}$ . This mass includes 740 kg for the Microsat-R satellite and 10 kg (estimated) for the kill vehicle. We use 100 logarithmically spaced  $L_c$  bins between 3 mm and 1 m, and with Equation 7 obtain a number distribution as a function of size for the generated debris fragments.

The logarithm of A/M ratios are sampled from unique probability distribution functions for each size, which are linear combinations of normal distributions detailed in the NSBM. The weights, means, and standard deviations for those distributions are functions of  $\log_{10}(L_c)$  and depend on the size regime of the fragment. For large fragments with  $L_c > 11 \text{ cm}$ , the PDF is bimodal, small fragments with  $L_c < 8 \text{ cm}$  are normally distributed, and sizes between these two regimes incorporates a transition function that is a linear combination of the two previous PDFs. These PDFs are sampled to obtain a distribution of A/M ratios. The area and mass for the fragment is obtained using its A/M ratio and equations (42a,b) of [15]. The initial number distribution  $\Delta N(L_c)$  is normalized using the ratio of the target payload mass to the total fragment mass  $m_t/m_{\text{frag,tot}}$ , the A/M and mass distributions are re-sampled, and this process is done iteratively until  $m_{\text{frag,tot}} \leq M_e$ , resulting in a total number of fragments  $N_{\text{tot}}$  and an updated mass of fragments  $M_e^* = m_{\text{frag,tot}}$ .

This process yields a number of fragments that is  $\mathcal{O}(10^5)$ , an unrealistic amount for long-term integration. We thus perform integrations of a sampling of 1,000 fragments. A few simulations were executed with 5,000 fragments as well to confirm that 1,000 gives a representative parameter set. These fragments are sampled from the distribution of A/M ratios that results from the above process. Using these A/M ratios, the NSBM gives a unique normal probability distribution of  $\log_{10}(\Delta v)$  for each fragment  $i$  with a mean  $\mu = 0.9 \log_{10}(A/M)_i + 2.9$  and standard deviation  $\sigma = 0.4$  (using mks units). A value is sampled for each fragment from its unique PDF to obtain a distribution of  $\Delta v$ 's for the fragments. These magnitudes are combined with a unit vector generated randomly from a uniform distribution in between -1 and 1 for each component, resulting in the final velocity kicks. In order to perform one simulation which implements a full NSBM number distribution rather than a sampling, we also simulate a debris cloud using 100 characteristic length bins between 10 cm and 1 m. The size of 10 cm also represents the approximate lower limit to the size of most trackable debris in LEO (although with technological advances in radar detection, this bound is improving towards fragment sizes of  $\mathcal{O}(1 \text{ cm})$ ).

Our generated values for A/M ratio and  $\Delta v$ 's are then integrated in REBOUND and their collision probabilities recorded, as outlined in Section 2.4.

### 2.3.2 Rayleigh Distribution

In this simplified method, we assume that the magnitudes of the fragment velocity kicks approximately follows a Rayleigh Distribution. We further fix the A/M ratio and the total number of fragments in the simulation, sidestepping any need to assign characteristic lengths or specific fragment masses. To compare this method with the NSBM, we perform simulations with both 1,000 fragments and the number of fragments that results from the mass-normalized number distribution using Equation 7 with  $L_c \in [0.1, 1.0]$  (unit of metres implied).

We set the mode of the Rayleigh distribution to  $\sigma = 250 \text{ m/s}$  and draw from the distribution for the magnitude of the velocity kicks, which produces a reasonable correspondence to the actual Gabbard plot of the India ASAT test. A

randomly oriented unit vector is assigned to each fragment, as in the NSBM. The fragments are added to a REBOUND simulation and integrated using the same process as described in the following section.

In this method,  $A/M = 0.1 \text{ m}^2\text{kg}^{-1}$  for all particles, unless stated otherwise.

## 2.4 Debris Integration

Table 2 lists the orbital parameters that we use for Microsat-R, the satellite destroyed in the India ASAT test. For each REBOUND simulation, the fragments are initialized with these orbital parameters, mimicking the instantaneous moment just prior to the collision. Each fragment is then perturbed following  $\mathbf{v} = \mathbf{v}_0 + \Delta\mathbf{v}$ , where  $\mathbf{v}_0$  is Microsat-R's approximate velocity just before the collision and  $\Delta\mathbf{v}$  is a fragment's respective velocity kick.

Table 2: Orbital parameters of Microsat-R just prior to the India ASAT test [16].

Altitude of ASAT test	283 km
Perigee	267.4 km
Apogee	288.7 km
Inclination	96.6°
Period	89.9 minutes
Semi-major axis	6649 km

In addition to gas drag, we include the Earth's  $J_2$  and  $J_4$  components. When the simulations are initialized, the  $\beta$  coefficients for gas drag are calculated from the  $A/M$  ratio distribution for all fragments using  $\beta = C_D A/M$ . For the Rayleigh distribution,  $\beta = 0.22$  for all fragments. At the start of a simulation, a desired satellite density field (see Section 2.2) is selected and read into REBOUND. The fragments are then integrated until either all the fragments have de-orbited or the simulation reaches two years of integration, whichever happens first. After every 30 minutes in the simulation, REBOUND removes particles that have decayed below a threshold altitude, which we set to 200 km.

When a fragment de-orbits, its cumulative collision probability  $\lambda$  is recorded for evaluating the total collision probability  $P_{coll}$ . Likewise, after two years of integration time, any remaining fragments also have their  $\lambda$ 's included in the calculation of  $P_{coll}$ .

For a particular satellite density field, the collision probability scales approximately linearly with the number of fragments, provided that the number of fragments adequately samples the full fragment distribution. This is the case with the simulations run here, which was verified by running identically seeded simulations with  $N_{\text{frags}} = (1, 2, 3, 4, 5) \times 10^3$  for both the NSBM and Rayleigh methods. For any simulation, we can thus scale the cumulative collision probability of a simulated sub-sample of fragments by the total number of fragments that would result from an entire NSBM number distribution.

## 3. RESULTS

Using the NSBM for  $3 \text{ mm} < L_C < 1 \text{ m}$  yields more than 300,000 debris fragments, with the majority of these below a few centimetres in size. This is consistent with other studies of Mission Shakti [5, e.g.], which find debris numbers of order  $10^5$  for sizes greater than 1 mm. The NSBM gives a re-normalized fragment number of  $N_{\text{frag}} = 1168$  for  $L_{c,\text{min}} = 10 \text{ cm}$ . While this value is significantly smaller than including sizes down to 3 mm, it is noteworthy that the consequences of  $> 10 \text{ cm}$  fragments colliding with a spacecraft will be much more consequential than that of a millimetre-sized fragment, and so while the lower number value for  $L_{c,\text{min}} = 10 \text{ cm}$  may yield a lower collision probability, the result of the collision itself is expected to be of higher significance.

Figure 1 shows Gabbard plots for three fragmentation models. The left panel is for an NSBM simulation with  $L_{c,\text{min}} = 10 \text{ cm}$ , while the middle panel is for the Rayleigh method with a total number of fragments set to match the model on the left. Both panels are for the debris immediately following the modelled fragmentation event. Only fragments with apogees below 2,500 km are shown for comparison with the right panel, which shows data from the India ASAT test<sup>4</sup>.

<sup>4</sup>Data are the first available TLE for each particle, as provided by USSPACECOM.

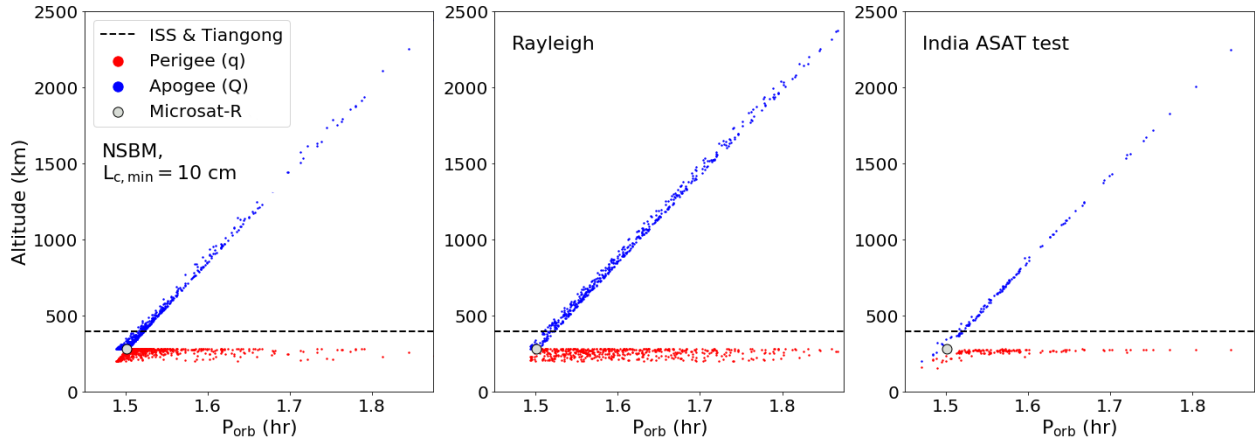


Fig. 1: Gabbard plots for low-altitude kinetic ASAT tests. From left to right, the plots show the initial state of the NSBM simulation with  $L_{c,\min} = 10$  cm, the Rayleigh  $\Delta v$  distribution, and the actual fragment data from the 2019 India ASAT test, based on the first available TLE for each fragment (data: USSPACECOM). Fragment apogees are shown in blue, and the perigees in red. The altitude of the International Space Station and China’s Tiangong space station is shown as a dashed line (note: this is intended to delineate altitude, only). The orbital period and altitude of Microsat-R satellite at the time of the India ASAT test are shown as the grey point.

Many of these fragments first appear in the satellite/debris catalogue well after the ASAT was conducted and therefore already include substantial orbital evolution due to gas drag. Thus, some differences in comparison with the other two panels are expected. As their orbits evolve, the fragments migrate toward the bottom left corner of the plot, as can be seen in the smattering of points in the bottom left of the India ASAT plot.

Figure 2 shows the fraction of fragments that have de-orbited as a function of time. Only fragments that de-orbit after the first five days are included to focus on long-lasting debris. Four different simulation results are shown: the NSBM simulations with lower characteristic lengths of 3 mm and 10 cm, and two simulations using Rayleigh distributions, one with a constant  $A/M = 0.1 \text{ m}^2 \text{ kg}^{-1}$  and another with  $A/M = 0.03 \text{ m}^2 \text{ kg}^{-1}$  (models A/M0.1 and A/M0.03, respectively). These are all compared with the actual de-orbit times for the tracked Microsat-R debris.

The fragments in the two NSBM and the Rayleigh A/M0.1 simulations completely de-orbit before the end of two years. In contrast, the Rayleigh A/M0.03 simulation still has 3.5% of the fragments remaining in orbit at the end of the two-year integration period, and a much lower overall slope in the de-orbit fraction. This result visualizes the sensitivity of the simulations to the A/M ratio distribution, all other things being equal. For reference, the peaks of the A/M ratio distributions in the NSBM models range from 0.1 to  $0.5 \text{ m}^2 \text{ kg}^{-1}$ , depending on  $L_{c,\min}$ . Fragments that were ejected into hyperbolic orbits are not included in the de-orbit fraction, but are worth noting. The NSBM  $\Delta v$  distribution has a high velocity tail, especially for simulations with the lower  $L_{c,\min}$  value of 3 mm. While relatively rare, the hyperbolic trajectories tended to occur in the NSBM for sizes at or below 1 cm. For example, 20 out of 1,000 fragments were ejected from Earth orbit in the  $L_{c,\min} = 3$  mm NSBM simulation. The Rayleigh distributions did not show this behaviour.

In comparison with the India ASAT test at face value, both NSBM simulations and the Rayleigh A/M0.1 models have shorter de-orbit timescales than what is catalogued for the Microsat-R debris. It must be kept in mind that the data are biased, in part, by the latency in identifying the debris from Microsat-R. For example, only about half of the fragments that were eventually catalogued by USSPACECOM were identified within approximately two weeks following the event. Thus, substantial evolution of the fragment ensemble, including de-orbits, likely occurred before their identification. The catalogued fragments are also incomplete. Nonetheless, these biases do not necessarily account for Microsat-R debris having an overall longer de-orbit timescale than what we see in our simulations. This suggests, for example, that a higher effective energy than what we use for the collision might be required when employing the NSBM (which is plausible), or as we showed, a slightly lower A/M ratio is needed for the debris, as highlighted by the Rayleigh models.

We stress that the simulations are not intended to reproduce exactly the India ASAT test; rather the comparison is

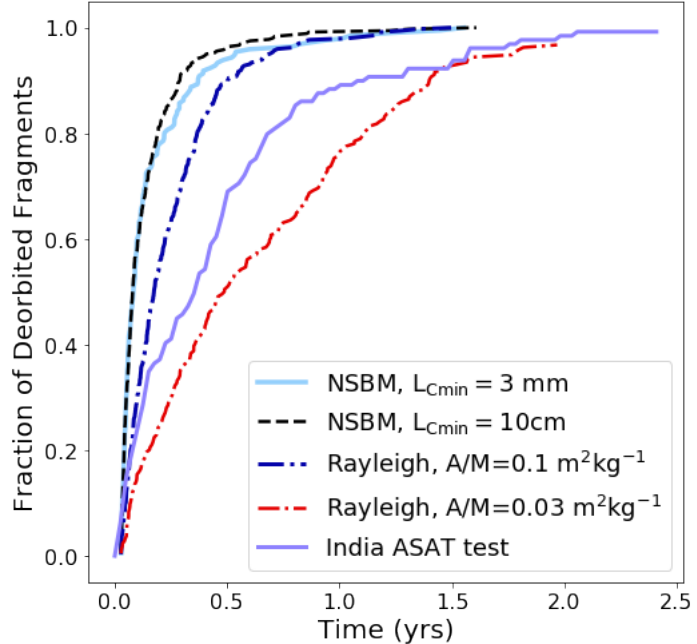


Fig. 2: The fraction of de-orbited fragments as a function of time. Simulations using 1,000 fragments and the NSBM with  $L_{c,\min} = 3$  mm and 10 cm are shown in solid light blue and dashed black lines, respectively. Two Rayleigh-method simulations are also shown, our standard simulation with 1,000 fragments and  $A/M = 0.1 \text{ m}^2\text{kg}^{-1}$  (dash-dotted dark blue curve), as well as a lower-resolution model with 500 fragments and  $A/M = 0.03 \text{ m}^2\text{kg}^{-1}$  (red dash-dotted line), which was done to demonstrate the sensitivity of the de-orbit times to the  $A/M$  ratio. In this last case, a few fragments last until the end of the integration time, which is set at two years. The re-entry data for India ASAT test fragments, as given in the USSPACECOM catalogue, are shown as a purple solid line.

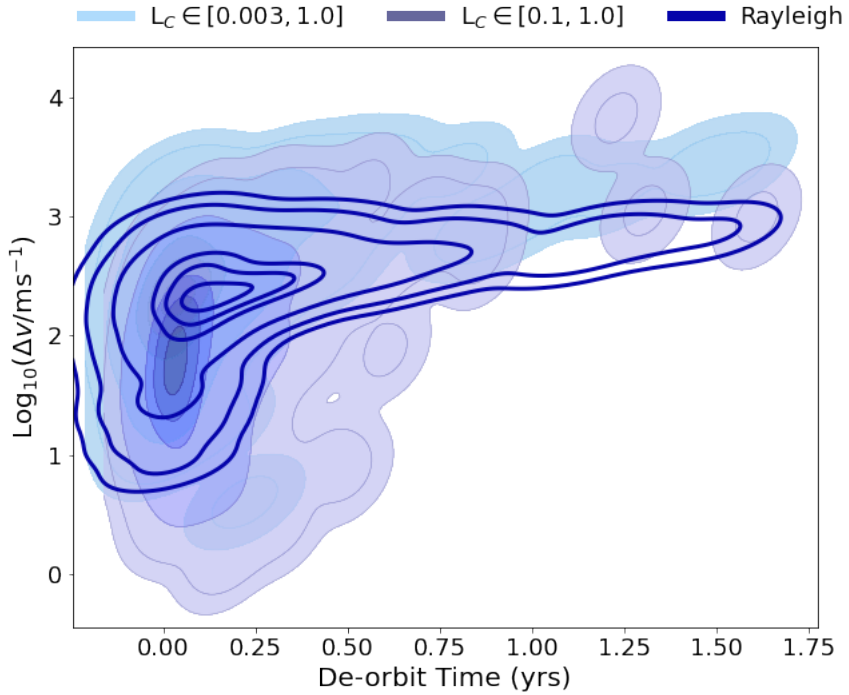


Fig. 3: The fragments'  $\Delta v$  velocity kicks shown against their de-orbit times. Contours represent 0.1%, 1%, 10%, 50%, 70%, 90%, and 100% of the fragments for each fragmentation model. The NSBM simulations for  $L_{c,\min} = 3$  mm and 10 cm are shown in the light and medium blue shading, respectively. Each simulation includes a sample of 1,000 fragments. The Rayleigh distribution's contours are shown in dark blue (without fill) and uses 1000 fragments. Only fragments that de-orbit past one day are shown. The majority of fragments deorbit in under six months, especially those with low velocity kicks whose orbits remain at low altitudes and eccentricities.

intended to show the plausibility and relevance of the models we explore. The faster de-orbit times seen in the simulations, again at face value, suggest that the collision probabilities derived from them underestimate the collision probability that was posed by the India ASAT test.

The relation between velocity kicks and de-orbit timescales is shown in Figure 3. The contours for each simulation represent seven levels between 0.1% and 100% of  $\log_{10}(\Delta v)$ . Only fragments with  $t_{\text{deorbit}} > 1$  day are included in this plot. As expected, most fragments de-orbit within the first few months following the ASAT test. This effect is exaggerated for the NSBM, with fragments at the extremes of the velocity kicks de-orbiting quickly and adding to the overall short-term de-orbit fraction like that seen in Figure 2. The  $\Delta v$  distributions cluster between  $10^2 - 10^3$  m/s for the NSBM simulation with  $L_c \in [0.003, 1.0]$ . The mode of the Rayleigh distribution overlaps the NSBM distribution, although the NSBM extends to higher  $\Delta v$  values, which is consistent with the differences in the models. The NSBM simulation with  $L_c \in [0.1, 1.0]$  also shows a concentration of  $\Delta v$  values around 50 to 150 m/s. Again, in the NSBM, larger fragments tend to have lower A/M ratios, and hence lower  $\Delta v$  values on average, as can be seen from the PDFs described in Section 2.3.1.

The probability of one or more collisions between satellites and ASAT fragments over the orbital lifetime of the ASAT debris is shown in Table 3. The leftmost column lists each simulation and its corresponding fragmentation model. This is followed by the results for three different satellite density fields, as described in Section 2.2. For each satellite density field, the collision probability is listed as determined directly from the sample size of 1,000 fragments. The probability is further scaled to account for the number of fragments predicted by the NSBM above a given size limit, as follows:

$$P_{\text{coll}} = 1 - \exp\left(-\frac{N_{\text{NSBM}}}{N_{\text{sim}}} \Lambda\right), \quad (9)$$

where  $N_{\text{sim}} = 1000$  for all sims in the table. As noted in Section 2.4, this scaling is possible because the number of

Table 3: Collision Probabilities

<b>Model</b>	<b>2019 sats</b>		<b>12,000 sats</b>		<b>65,000 sats</b>	
	$P_{coll}$ $N_{sample}=1000$	scaled	$P_{coll}$ $N_{sample}=1000$	scaled	$P_{coll}$ $N_{sample}=1000$	scaled
NSBM, $L_{c,min} = 0.1$ m	0.04%	0.05%	0.40%	0.47%	1.9%	2.2%
Rayleigh, $N(L_{c,min} = 0.1$ m)	0.13%	0.15%	0.67%	0.78%	3.1%	3.6%
NSBM, $L_{c,min} = 0.003$ m	0.03%	10%	0.18%	45%	0.85%	94%
Rayleigh, $N(L_{c,min} = 0.003$ m)	0.13%	35%	0.67%	89%	3.1%	100%

fragments in the simulations adequately sample the NSBM distribution functions. Recall that the Rayleigh models do not inherently rely on particle size, so the NSBM numbers are used for their scaling as well. The similarity between the unscaled and the scaled values for cases that use  $L_{c,min} = 0.1$  m arises because the number of fragments in that model is close to the 1,000 used in the simulations. There is also a difference in the unscaled probabilities between the two NSBM models. In the realizations studied, the  $L_{c,min} = 0.003$  m model happens to have a higher fraction of particles that de-orbit right away, which gives rise to the lower unscaled number. Together, the different distributions give insight into the range of outcomes we might expect.

The increase in collision probability from the LEO environment in 2019 to a present-day satcon environment is significant; in some cases as much as two orders of magnitude higher. The sheer number of fragments for sizes down to 3 mm guarantees that a collision of some form will occur, although these may not lead to significant spacecraft damage.

To explore this further, we run a higher resolution simulation with 5000 fragments for an NSBM with  $L_{c,min} = 3$  mm. We find that the scaled  $P_{coll}$  is 92% for fragments between  $L_c = 3$  mm and 1 cm in size, 33% for  $L_c > 1$  cm, about 6% for  $L_c \gtrsim 5$  cm, and about 3% for  $L_c \gtrsim 10$  cm (these are consistent to a few% of the values shown in Table 3). That is, although the most likely collision to happen is with a small fragment, the probability that a fragment of sufficient size to prompt additional fragmentation events is non-negligible for ASAT tests similar to those modelled here.

#### 4. SUMMARY AND DISCUSSION

In this study, we simulated the evolution of debris produced in kinetic ASAT tests, similar to the 2019 India test, and evaluated the probability that such events would lead to collisions with satellites. Different satellite density fields were explored, including different populations of large satellite constellations (satcons).

Debris fragments were integrated using the REBOUND astrodynamics code to assess the collision probabilities for different fragmentation models. This includes the NASA Standard Breakup Model (NSBM), and a simplified, but instructive Rayleigh velocity distribution model with a constant A/M ratio.

For the fragmentation models that we explored, we found de-orbit timescales that tended to be faster than what was seen with the India 2019 event. As such, the fragmentation events that we explore are not only plausible ASAT events, but may underestimate the risks to orbital infrastructure of such behaviour.

When using the NSBM, we found that there is  $> 90\%$  probability for fragments with sizes  $L_c > 3$  mm to impact one or more satellites in the 65,000 satellite satcon environment. The 12,000 satellite satcon environment is also high, with a collision probability of about 45%. These probabilities are both much more significant than that for the 2019 satellite population, which, while non-negligible, is about 10%. Although these impacts do not necessarily mean that they will

result in subsequent fragmentation events, they are nonetheless cause for concern.

When focusing on size scales of  $L_c > 1$  cm and  $L_c > 10$  cm in the NSBM model, we found that the 65,000 satellite environment still has an approximate 30% and 2% to 3% chance, respectively, of experiencing one or more collisions, with the latter of particular concern for prompting subsequent large fragmentation events.

With this in mind, the risks associated with non-catastrophic collisions should not be dismissed, as even small fragmentation events contribute to the overall debris population, including non-tracked debris.

When comparing the two fragmentation methods used here, we see a larger collision probability for the Rayleigh velocity distribution than for the NSBM. However, the Rayleigh A/M0.1 model happens to produce fragments with a slightly longer de-orbit timescale than what occurs when using the NSBM. This just emphasizes the consequences of long-lived debris.

When interpreting the results, it is important to keep several caveats in mind. First, the satellite density fields are based on plausible satcon configurations, but these are continuously changing. Nonetheless, because ASAT tests will tend to spread fragments over a wide range of altitudes in LEO, the collision rates can be expected to scale with the number of satellites.

Second, we assumed a fixed cross sectional area for each satellite of  $10 \text{ m}^2$ . The collision rate will again be proportional to the average satellite cross section in each orbital shell. If all shells have comparable satellites, then the expected number of collisions will scale directly with the actual cross section.

Finally, we only focused on one type of kinetic ASAT, modelled after the 2019 India kinetic ASAT test. We thus did not explore an extensive range of parameter space that is available to ASATs. Regardless, we focused on results from simulations that had an overall de-orbit timescale that is shorter than the actual India ASAT.

Overall, the results demonstrate that debris-generating ASAT tests are incompatible with providing a safe operating environment in LEO, and are particularly dangerous in a heavily commercialized operating environment. Even events that ensure that fragments de-orbit in less than a year can cause dangerous levels of collisional risk and threaten the continued use and development of LEO by all space users.

This work was supported in part by the University of British Columbia, the Canada Research Chairs program, a Natural Sciences and Engineering Research Council Discovery grant, and a grant from the Tri-agency New Frontiers in Research Fund.

## REFERENCES

- [1] M. Langbroek, The Diplomat, April (2019). <https://thediplomat.com/2019/05/why-indias-asat-test-was-reckless/>.
- [2] R. Chaundry, The Economic Times, March (2019). <https://economictimes.indiatimes.com/news/politics-and-nation/explained-whats-mission-shakti-and-how-was-it-executed/articleshow/68607473.cms>
- [3] A. Tellis, Carnegie Endowment for International Peace, April (2019). <https://carnegieendowment.org/2019/04/15/india-s-asat-test-incomplete-success-pub-78884>
- [4] L. Grush, The Verge, August (2019). <https://www.theverge.com/2019/8/8/20754816/india-asat-test-mission-shakti-space-debris-tracking-air-force>
- [5] Y. Jiang, *Helyion*, Vol 6, 8 (2020). <https://doi.org/10.1016/j.heliyon.2020.e04692>
- [6] D. Kessler and B. Cour-Palais, *JGR Space Physics*, Vol. 83, 2637-2646 (1978). <https://doi.org/10.1029/JA083iA06p02637>
- [7] Federal Communications Commission. IBFS, SAT-LOA-20161115-00118, Attachment A (2016).
- [8] Federal Communications Commission. IBFS, SAT-LOA-20170301-00027, Attachment A (2017).
- [9] Federal Communications Commission. IBFS, SAT-MOD-20200417-00037, Attachment A (2020).
- [10] Federal Communications Commission. IBFS, SAT-LOA-20200526-00055, Attachment A (2020).
- [11] Federal Communications Commission. IBFS, SAT-MPL-20210112-00007, Attachment A (2021).
- [12] H. Rein and D. Spiegel. *MNRAS*, vol 446, 2, 1424-1437 (2015). <https://doi.org/10.1093/mnras/stu2164>

- [13] H. Rein and D. Tamayo. *MNRAS*, vol 452, 1, 376-388 (2015). <https://doi.org/10.1093/mnras/stv1257>
- [14] COSPAR International Reference Atmosphere– 2012. “CIRA-2012, Models of the Earth’s Upper Atmosphere”, technical report, chapters 1 to 3. [https://spacewx.com/wp-content/uploads/2021/03/chapters\\_1\\_3.pdf](https://spacewx.com/wp-content/uploads/2021/03/chapters_1_3.pdf)
- [15] S. Frey and C. Colombo. *Journal of Guidance, Control, and Dynamics*, vol 44, 1 (2021). <https://doi.org/10.2514/1.G004939>
- [16] Great Game India. “Mission Shakti – India’s Anti-Satellite Missile Test Wiki”, *Journal on Geopolitics and International Relations*, March (2019). <https://greatgameindia.com/mission-shakti-indias-anti-satellite-missile-test>
- [17] L. Press. “A New Chinese Broadband Satellite Constellation”, CircleID, October (2020). <https://circleid.com/posts/20201002-a-new-chinese-broadband-satellite-constellation>
- [18] Federal Communications Commission. IBFS, SAT-LOA-20190704-00057, Technical Appendix (2019).